Numerical investigation of an orthotropic finite elasticity problem using a constrained minimization theory to prevent material overlapping

Lucas A. Rocha[1], Adair R. Aguiar[1]

[1]*Department of Structural Engineering, São Carlos School of Engineering, University of São Paulo*
Av. Trabalhador Sãocarlense, 400, Cx. P. 359, 13560-590, São Carlos-SP, Brazil
lucas.almeida.rocha@usp.br, aguiarar@sc.usp.br

Abstract. We consider the equilibrium of an annular disk that is fixed on its inner surface and subjected to uniform pressure on its outer surface. The disk is cylindrically orthotropic and radially reinforced, which may be found in certain types of woods and carbon fibers with radial microstructure. In the context of the classical linear elasticity, the solution of this problem predicts material overlapping. A way to prevent this unphysical behavior consists of using a constrained minimization theory together with classical nonlinear elasticity. Another way consists of adopting a material model that is adequate for large deformations. In this work, we compare both of these approaches and obtain solutions that are in very good agreement with each other. In addition, these solutions yield discontinuous deformation gradients. This creates numerical difficulties, which are overcome by including the position of a discontinuity as a variable of the numerical procedure. This research is of interest in the study of stress-induced phase transformations.

Keywords: Nonlinear elasticity, Orthotropy, Constrained Minimization, Local injectivity constraint, Finite element method

1 Introduction

Certain problems in classical linear elasticity have solutions that predict material overlapping for a small external load, which is not physically acceptable. One such problem concerns the equilibrium of an annular disk that is fixed on its inner surface of radius R_i and is subjected to a uniform pressure on its outer surface of radius R_e. The disk is cylindrically orthotropic and radially reinforced, in the sense that the disk is stiffer in the radial direction than in the tangential direction. Material properties of this type are found in certain types of woods [1] and carbon fibers with radial microstructure [2].

To avoid material overlapping, Fosdick and Royer-Carfagni [3] have proposed to minimize the energy functional $\mathcal{E}$ of classical linear elasticity subject to the local injectivity constraint $\det \mathbf{F} \geq \varepsilon > 0$, where $\mathbf{F}$ is the deformation gradient and ε is a small positive parameter. Even though material overlapping is eliminated, the theory still predicts that large deformations, which violate the hypothesis of infinitesimal strains of the linear theory, still occur. In previous works [4, 5], we have extended this constrained theory to the nonlinear elasticity theory by considering that $\mathcal{E}$ is the energy functional of a hyperelastic material. As we will see in Section 4, a distinguishing feature this nonlinear constrained minimization theory is that, for the disk problem, it yields a bounded Lagrange multiplier field, whereas its linear counterpart yields an unbounded one when $\varepsilon \to 0$.

Another way to prevent material overlapping consists of adopting a material model that is adequate for large deformations. In this work, we compare these two approaches. For this, we investigate the disk problem using two different models. The first model concerns the orthotropic St Venant-Kirchhoff model in the context of the above constrained minimization theory. The second model concerns a compressible Mooney-Rivlin model [6] that is extended to the orthotropic case as proposed by Bonet and Burton [7]. For this second model, we do not impose the local injectivity constraint explicitly since the model is conceived to satisfy this constraint implicitly. In addition, the solutions obtained with both models have a discontinuity in the deformation gradient when the pressure is large enough. This creates numerical difficulties, which are overcome by including the position of this discontinuity as a variable of the numerical procedure. Therefore, the numerical procedure used in this work is of interest in the study of stress-induced phase transformations, where the deformation field is typically not smooth.

In Section 2, we formulate the disk problem for both material models. In Section 3, we present the numerical procedure used to obtain the numerical results presented in Section 4. In Section 5, we present some concluding

remarks.

2 The disk problem

Let $\mathcal{B} \subset \mathbb{R}^3$ denote the undistorted reference configuration of a homogeneous annular disk in equilibrium. The disk has an inner radius $R_i > 0$, outer radius $R_e > R_i$ and unitary thickness. Points $\mathbf{x} \in \mathcal{B}$ are mapped into points $\mathbf{y} \triangleq \mathbf{f}(\mathbf{x}) = \mathbf{x} + \mathbf{u}(\mathbf{x})$, where $\mathbf{f}$ and $\mathbf{u}$ are the deformation and the displacement fields, respectively. The boundary $\partial\mathcal{B}$ of $\mathcal{B}$ is composed of two non-intersecting parts, $\partial_1\mathcal{B}$ and $\partial_2\mathcal{B}$, which represent the inner and outer surfaces of the disk, respectively. The disk is fixed on $\partial_1\mathcal{B}$ so that $\mathbf{f} = \mathbf{x}$ on $\partial_1\mathcal{B}$. On $\partial_2\mathcal{B}$, there is a pressure load $\bar{\mathbf{t}}$, which is constant in the deformed configuration and given by $\bar{\mathbf{t}} = -p \operatorname{cof} \mathbf{F}\, \mathbf{N}$, where $p > 0$, $\operatorname{cof} \mathbf{F} \triangleq (\det \mathbf{F})\, \mathbf{F}^{-T}$, $\mathbf{N}$ is the outward unit normal to $\partial_2\mathcal{B}$, and $\mathbf{F} \triangleq \nabla \mathbf{f} = \mathbf{I} + \nabla \mathbf{u}$, with ∇ denoting the gradient operator with respect to $\mathbf{x}$ and $\mathbf{I}$ denoting the identity tensor.

Let $\{\mathbf{e}_R, \mathbf{e}_\Theta, \mathbf{e}_Z\}$ denote the usual orthonormal cylindrical basis at $\mathbf{x}$ associated with the cylindrical coordinates (R, Θ, Z), such that $\mathbf{x} = R\, \mathbf{e}_R(\Theta) + Z\, \mathbf{e}_Z$. Similarly, let $\{\mathbf{e}_r, \mathbf{e}_\theta, \mathbf{e}_z\}$ and (r, θ, z) be the corresponding orthonormal cylindrical basis and coordinates, respectively, at $\mathbf{y}$, such that $\mathbf{y} = r\, \mathbf{e}_r(\theta) + z\, \mathbf{e}_z$. Unless stated otherwise, we shall omit the dependence of $\mathbf{e}_R$ and $\mathbf{e}_r$ on Θ and θ, respectively.

The disk is made of a cylindrically orthotropic material. We consider two hyperelastic models for the disk. The first model concerns an orthotropic St Venant-Kirchhoff material, which is a natural extension from the classical linear elastic material. The second model is a compressible Mooney-Rivlin material model [6] extended to the orthotropic case, as proposed by Bonet and Burton [7]. The strain energy functions of the models are given by

$$\begin{aligned} \bar{W}_{\mathrm{vk}}(I_1, I_2, I_4, I_5, I_6, I_7) &= \bar{W}^{\mathrm{iso}}_{\mathrm{vk}}(I_1, I_2) + \bar{W}_{\mathrm{aniso}}(I_1, I_4, I_5, I_6, I_7)\,, \\ \bar{W}^{\mathrm{iso}}_{\mathrm{vk}}(I_1, I_2) &= \mu\,(I_1 - 3) + \frac{\lambda + 2\,\mu}{8}(I_1 - 3)^2 - \frac{\mu}{2}\,(I_2 - 3)\,, \end{aligned} \tag{1}$$

$$\begin{aligned} \bar{W}_{\mathrm{mr}}(I_1, I_2, I_4, I_5, I_6, I_7) &= \bar{W}^{\mathrm{iso}}_{\mathrm{mr}}(I_1, I_2, I_3) + \bar{W}_{\mathrm{aniso}}(I_1, I_4, I_5, I_6, I_7)\,, \\ \bar{W}^{\mathrm{iso}}_{\mathrm{mr}}(I_1, I_2, I_3) &= a\,(I_1 - 3) + b\,(I_2 - 3) + c\,(I_3 - 1) - \frac{d}{2}\,\log I_3\,, \end{aligned} \tag{2}$$

$$\begin{aligned} \bar{W}_{\mathrm{aniso}}(I_1, I_4, I_5, I_6, I_7) = \frac{1}{4}\Big[&\alpha_1\,(I_4 - 1)^2 + \alpha_2\,(-2\,I_4 + I_5 + 1) + \alpha_3\,(I_1 - 3)\,(I_4 - 1) + \alpha_4\,(I_6 - 1)^2 \\ &+ \alpha_5\,(-2\,I_6 + I_7 + 1) + \alpha_6\,(I_1 - 3)\,(I_6 - 1) + \alpha_7\,(I_4 - 1)\,(I_6 - 1)\Big]\,, \end{aligned} \tag{3}$$

where the subscripts "vk" and "mr" denote the St Venant-Kirchhoff and Mooney-Rivlin materials, respectively, μ, λ, a, b, c, d, α_i, $i = 1, 2, 3, ..., 7$, are material parameters, and I_i, $i = 1, 2, 3, ..., 7$, are given in terms of the right Cauchy-Green strain tensor $\mathbf{C} = \mathbf{F}^T\,\mathbf{F}$ by

$$\begin{aligned} &I_1 \triangleq \operatorname{tr} \mathbf{C}\,, \qquad I_2 \triangleq \frac{1}{2}[I_1^2 - \operatorname{tr}(\mathbf{C}^2)]\,, \qquad I_3 \triangleq \det \mathbf{C}\,, \\ &I_4 \triangleq \mathbf{m}_1 \cdot \mathbf{C}\,\mathbf{m}_1\,, \quad I_5 \triangleq \mathbf{m}_1 \cdot \mathbf{C}^2\,\mathbf{m}_1\,, \quad I_6 \triangleq \mathbf{m}_2 \cdot \mathbf{C}\,\mathbf{m}_2\,, \quad I_7 \triangleq \mathbf{m}_2 \cdot \mathbf{C}^2\,\mathbf{m}_2\,. \end{aligned} \tag{4}$$

The vectors $\mathbf{m}_1$ and $\mathbf{m}_2$ are the material symmetry directions, which, in this work, are given by $\mathbf{m}_1 = \mathbf{e}_R$ and $\mathbf{m}_2 = \mathbf{e}_\Theta$. Additionally, in order for the response of the above hyperelastic models to reduce to that of a linearly elastic material under infinitesimal deformations, their material parameters are related to the classical elasticity constants by the relations

$$\begin{aligned} &\lambda = c_{33} - 2\,(c_{44} + c_{55} - c_{66})\,, && \mu = c_{44} + c_{55} - c_{66}\,, \\ &a = c - \frac{c_{33}}{4} + c_{44} + c_{55} - c_{66}\,, && b = -c + \frac{c_{33}}{4} - \frac{1}{2}\,(c_{44} + c_{55} - c_{66})\,, \qquad d = \frac{c_{33}}{2}\,, \\ &\alpha_1 = \frac{c_{11}}{2} - c_{13} + \frac{c_{33}}{2} - 2\,c_{55}\,, && \alpha_2 = 2\,(-c_{44} + c_{66})\,, \\ &\alpha_3 = c_{13} - c_{33} + 2\,(c_{44} + c_{55} - c_{66})\,, && \alpha_4 = \frac{c_{22}}{2} - c_{23} + \frac{c_{33}}{2} - 2\,c_{44}\,, \\ &\alpha_5 = 2\,(-c_{55} + c_{66})\,, && \alpha_6 = c_{23} - c_{33} + 2\,(c_{44} + c_{55} - c_{66})\,, \\ &\alpha_7 = c_{12} - c_{13} - c_{23} + c_{33} - 2\,(c_{44} + c_{55} - c_{66})\,. \end{aligned} \tag{5}$$

We want to find a deformation field $\mathbf{f}$, such that points $\mathbf{x} = (R, \Theta, Z) \in [R_i, R_e] \times [0, 2\pi] \times [0, 1]$ move along radial lines according to

$$\mathbf{f}(R, \Theta, Z) = r(R)\, \mathbf{e}_r(\Theta) + Z\, \mathbf{e}_z\,. \tag{6}$$

The corresponding displacement field has the form

$$\mathbf{u}(R,\Theta,Z) = u_r(R)\,\mathbf{e}_R\,, \qquad u_r(R) = r(R) - R\,. \tag{7}$$

Since $\mathbf{F} \triangleq \nabla\mathbf{f}$, we have that

$$\mathbf{F} = \nu(R)\,\mathbf{e}_r \otimes \mathbf{e}_R + \tau(R)\,\mathbf{e}_\theta \otimes \mathbf{e}_\Theta + \mathbf{e}_z \otimes \mathbf{e}_Z\,, \qquad \nu(R) \triangleq r'(R)\,, \quad \tau(R) \triangleq r(R)/R\,, \tag{8}$$

where the explicit dependence on $\mathbf{x} = (R,\Theta,Z)$ is omitted and $(\cdot)'$ denotes the derivative with respect to R.

In this work, we want to find the radial displacement field $u_r : (R_i, R_e) \to \mathbb{R}$ that minimizes the energy functional [6]

$$\check{\mathcal{E}}(u_r) \triangleq \mathcal{E}(\mathbf{f}) \triangleq \int_{\mathcal{B}} W(\mathbf{F})\,\mathrm{d}\mathbf{x} + \frac{p}{3}\int_{\partial\mathcal{B}} (\operatorname{cof}\mathbf{F}\,\mathbf{N})\cdot\mathbf{f}\,\mathrm{d}\mathbf{x}\,. \tag{9}$$

We refer to this problem as the disk minimization problem (*disk MP*). For the St Venant-Kirchhoff material, it follows from (1), (4), (5), (8), and (7.b), that $\check{\mathcal{E}}$ in (9) can be written as

$$\begin{aligned}\check{\mathcal{E}}^{\,\mathrm{vk}}(u_r) \triangleq \pi \int_{R_i}^{R_e} \Big(&\frac{c_{11}}{4}\,R\,{u_r'}^4 + c_{11}\,R\,{u_r'}^3 + c_{11}\,R\,{u_r'}^2 + c_{12}\,u_r\,{u_r'}^2 + 2\,c_{12}\,u_r\,u_r' \\ &+ \frac{c_{12}}{2\,R}\,u_r^2\,{u_r'}^2 + \frac{c_{12}}{R}\,u_r^2\,u_r' + \frac{c_{22}}{R}\,u_r^2 + \frac{c_{22}}{R^2}\,u_r^3 + \frac{c_{22}}{4\,R^3}\,u_r^4\Big)\,\mathrm{d}R \\ &+ \pi\,p\,\left[(R_e + u_r(R_e))^2 - R_i^2\right]\,.\end{aligned} \tag{10}$$

Similarly, for the Mooney-Rivlin material, we use (2) in place of (1) to write $\check{\mathcal{E}}$ as

$$\begin{aligned}\check{\mathcal{E}}^{\,\mathrm{mr}}(u_r) \triangleq \check{\mathcal{E}}^{\,\mathrm{vk}}(u_r) + \pi\,c_{33}\int_{R_i}^{R_e}\Bigg\{&-\frac{R\,{u_r'}^4}{4} - R\,{u_r'}^3 - \frac{R\,{u_r'}^2}{2} + R\,u_r' \\ &- \frac{R}{2}\,\log\left[\frac{(R^2 + 2\,R\,u_r + u_r^2)\,({u_r'}^2 + 2\,u_r' + 1)}{R^2}\right] \\ &+ u_r - \frac{u_r^2}{2\,R} - \frac{u_r^3}{R^2} - \frac{u_r^4}{4\,R^3}\Bigg\}\,\mathrm{d}R\,.\end{aligned} \tag{11}$$

Observe from (10) and (11) that $\check{\mathcal{E}}^{\,\mathrm{vk}}$ depends only on the elastic constants c_{11}, c_{22}, and c_{12}, whereas $\check{\mathcal{E}}^{\,\mathrm{mr}}$ depends also on c_{33}. In addition, for the St Venant-Kirchhoff material, we explicitly impose the local injectivity constraint $\det\mathbf{F} \geq \varepsilon > 0$, where ε is a small positive parameter. Without imposing this constraint, it is well known that this material may yield a deformation that predicts self-intersection. For the Mooney-Rivlin material, this constraint is not imposed explicitly because the model is conceived to satisfy this constraint implicitly.

3 Numerical procedure

We use a Finite Element formulation to find approximate minimizers of the disk MP. For this, let $\mathcal{V}_h$ be a finite dimensional space spanned by a set of basis functions $\{\mathbf{w}_i\}$, where h stands for the characteristic length of the finite element. Then, an approximate minimizer $\mathbf{u}_h \in \mathcal{V}_h$ can be written as

$$\mathbf{u}_h = u_h\,\mathbf{e}_R\,, \qquad u_h = \sum_{i=1}^{m} s_i\,w_i\,, \tag{12}$$

where $s_i \in \mathbb{R}$, $i = 1, 2, 3, ..., m$, is a degree of freedom and m is the number of degrees of freedom associated with the discretization. In this work, we use linear finite elements and a Gauss-Legendre quadrature rule with two points.

For both St Venant-Kirchhoff and Mooney-Rivlin materials, it follows from (1), (2), and (8) that the radial normal stress $P_{rr} \triangleq \mathbf{e}_r \cdot \mathbf{P}\,\mathbf{e}_R$, where $\mathbf{P} = \partial W/\partial\mathbf{F}$ is the first Piola-Kirchhoff stress tensor, is given by

$$P_{rr}(R) = \hat{P}_{rr}^{\,\mathrm{vk}}(\nu,\tau) = \left[c_{11}\,(\nu^2 - 1) + c_{12}\,(\tau^2 - 1)\right]\nu/2 \tag{13}$$

for the St Venant-Kirchhoff material and by

$$P_{rr}(R) = \hat{P}_{rr}^{\,\mathrm{mr}}(\nu,\tau) = \hat{P}_{rr}^{\,\mathrm{vk}}(\nu,\tau) - (\nu^4 - 2\,\nu^2 + 1)\,c_{33}\,/\,(2\,\nu) \tag{14}$$

for the Mooney-Rivlin material. It is possible to verify that, for a given τ, both $\hat{P}_{rr}^{\rm vk}$ and $\hat{P}_{rr}^{\rm mr}$ are non-monotonic with respect to ν depending on the elastic constants. These extrema occur for $\nu = \nu_{e1}$ and $\nu = \nu_{e2}$, where

$$\nu_{e1} = -\nu_{e2} = \frac{\sqrt{3}}{3}\sqrt{(-\tau^2 + \bar{\tau}^2)\,\frac{c_{12}}{c_{11}}}\,, \qquad \bar{\tau} \triangleq \sqrt{\frac{c_{11}+c_{12}}{c_{12}}} \tag{15}$$

for the St Venant-Kirchhoff material and

$$\nu_{e1} = \sqrt{\frac{-\bar{b} + \sqrt{\bar{b}^2 - 4\,\bar{a}\,\bar{c}}}{2\,\bar{a}}}\,, \qquad \nu_{e2} = \sqrt{\frac{-\bar{b} - \sqrt{\bar{b}^2 - 4\,\bar{a}\,\bar{c}}}{2\,\bar{a}}}\,, \tag{16}$$
$$\bar{a} \triangleq 3\,(c_{11} - c_{33})\,, \qquad \bar{b} \triangleq (\tau^2 - 1)\,c_{12} - c_{11} + 2\,c_{33}\,, \qquad \bar{c} \triangleq c_{33}$$

for the Mooney-Rivlin material.

In previous works [4, 8], we have verified that this non-monotonicity yields a discontinuity in the deformation gradient if the pressure is large enough. This discontinuity creates numerical difficulties, which can be overcome by using a numerical procedure that includes the position of the discontinuity $R = R_{\mathcal{S}}$ as an additional variable of the problem. Although these previous works concern only the St Venant-Kirchhoff material, the same behavior is expected for the Mooney-Rivlin material considered in this work; thus, here, we use a similar procedure.

This procedure requires the introduction of a penalizing functional. For the Mooney-Rivlin material, we define the functional

$$\mathcal{P}(u_r, R_{\mathcal{S}}) \triangleq \delta_e \left[\int_{\mathcal{B}_i} \max\left(0, \nu - \nu_{e2}\right)^2 \mathrm{d}\mathbf{x} + \int_{\mathcal{B}_e} \max\left(0, \nu_{e1} - \nu\right)^2 \mathrm{d}\mathbf{x}\right] \geq 0\,, \tag{17}$$

where both ν_{e1} and ν_{e2} are given by (16), $\delta_e > 0$ is a penalty parameter, $\mathcal{B}_i \triangleq \{\mathbf{x} \in \mathcal{B} \,|\, R_i < R < R_{\mathcal{S}}\}$, and $\mathcal{B}_e \triangleq \{\mathbf{x} \in \mathcal{B} \,|\, R_{\mathcal{S}} < R < R_e\}$. We see from the above equation that $\mathcal{P}$ is null if and only if $\nu \geq \nu_{e1}$ in $\mathcal{B}_e$ and $\nu \leq \nu_{e2}$ in $\mathcal{B}_i$. In addition, $R_{\mathcal{S}}$ is not limited to be in the interval $[R_i, R_e]$; for instance, $R_{\mathcal{S}} < R_i$ means that $\mathcal{B}_i = \emptyset$, $\mathcal{B}_e = \mathcal{B}$.

For the St Venant-Kirchhoff material, we also need to consider the local injectivity constraint, which is imposed by using an Augmented Lagrangian formulation. Then, we define the functional

$$\mathcal{L}(u_r, R_{\mathcal{S}}) \triangleq \int_{\mathcal{B}_i} \left(-\lambda\, c + \frac{\delta}{2}\, c^2\right) \mathrm{d}\mathbf{x} + \delta_e \int_{\mathcal{B}_e} \max\left(0, \nu_{e1} - \nu\right)^2 \mathrm{d}\mathbf{x}\,, \tag{18}$$

where $\delta > 0$ is a penalty parameter, ν_{e1} is given by (15), and $\lambda = \lambda(R)$ is the Lagrange multiplier field associated with the constraint $c \triangleq \det \mathbf{F} - \varepsilon = 0$ in $\mathcal{B}_i$.

The discrete version of the disk MP is given by the bi-level minimization problem

$$\min_{R_{\mathcal{S}} \in \mathbb{R}} \;\; \min_{\mathbf{s} \in \mathbb{R}^m} \mathcal{F}(\mathbf{s}, R_{\mathcal{S}})\,, \qquad \mathcal{F}(\mathbf{s}, R_{\mathcal{S}}) = \begin{cases} \mathcal{E}_h^{\rm vk}(\mathbf{s}) + \mathcal{L}_h(\mathbf{s}, R_{\mathcal{S}}) & \text{(St Venant-Kirchhoff material)} \\ \mathcal{E}_h^{\rm mr}(\mathbf{s}) + \mathcal{P}_h(\mathbf{s}, R_{\mathcal{S}}) & \text{(Mooney-Rivlin material)} \end{cases}, \tag{19}$$

where we have used (12) to introduce the vector $\mathbf{s} \triangleq (s_1, s_2, ..., s_m)$ and the functions $\mathcal{E}_h^{\rm vk}(\mathbf{s}) \triangleq \check{\mathcal{E}}^{\,\rm vk}(u_h)$, $\mathcal{E}_h^{\rm mr}(\mathbf{s}) \triangleq \check{\mathcal{E}}^{\,\rm mr}(u_h)$, $\mathcal{P}_h(\mathbf{s}, R_{\mathcal{S}}) \triangleq \mathcal{P}(u_h, R_{\mathcal{S}})$, and $\mathcal{L}_h(\mathbf{s}, R_{\mathcal{S}}) \triangleq \mathcal{L}(u_h, R_{\mathcal{S}})$. Observe from (19) that the inner level is a minimization problem in the vector variable $\mathbf{s}$ parameterized by $R_{\mathcal{S}}$ and that the outer level is a minimization problem in the scalar variable $R_{\mathcal{S}}$, which we solve by using the golden-section search.

We set the initial search interval of the golden-section search to be $[0.9\,R_i, 0.02\,R_e]$. At each iteration of this method, we solve the inner problem for a given $R_{\mathcal{S}}$ using a standard numerical procedure, which we comment more below. Then, we evaluate the corresponding $\mathcal{F}(\mathbf{s}, R_{\mathcal{S}})$ and proceed to the next iteration, where the search interval is reduced, as usual, in a golden-section search. We repeat these iterations until the search interval is smaller than a certain tolerance, which is equal to 10^{-6} in this work.

For the Mooney-Rivlin materials, we solve the inner problem by starting from an initial candidate $\mathbf{s} = \mathbf{s}_0$ and by using a standard Newton-Raphson method with a unidirectional search. For the St Venant-Kirchhoff material, we introduce a finite element approximation of λ given by

$$\lambda_h = \sum_{i=1}^{m_\lambda} l_i\, w_i\,, \tag{20}$$

where $l_i \in \mathbb{R}$, $i = 1, 2, 3, ..., m_\lambda$, is a degree of freedom, m_λ is the number of degrees of freedom associated with the approximation of λ, and w_i is a shape function of the finite element approximation. In this work, λ_h is

constant by parts, so that m_λ coincides with the number of mesh elements used in the discretization. Starting from $l_1 = l_2 = ... = l_{m_\lambda} = 0$ and $\mathbf{s} = \mathbf{s}_0$, we solve the inner problem using a standard Newton-Raphson method with a unidirectional search. Then, we update l_i, $i = 1, 2, 3, ..., m_\lambda$, as explained below and solve again the inner problem starting from the solution of the previous problem. We repeat this process until the L_2-norm of the update of λ_h is lower than 10^{-3}. We update l_i, $i = 1, 2, 3, ..., m_\lambda$, using the following recursive formula.

$$l_i^{(k+1)} = l_i^{(k)} - \delta\, c_i^{(k)}\,, \tag{21}$$

where the superscript denotes an iteration and $c_i^{(k)}$ is equal to c evaluated at the center of the i-th mesh element in the k-th iteration. For more details on the golden-section search, the Newton-Raphson method, the unidirectional search, and the augmented Lagrangian method, see, for instance, Luenberger and Ye [9].

4 Numerical results

We now use the numerical procedure presented in the previous section to obtain approximate solutions of the disk MP. We use a non-uniform mesh composed of 1536 elements distributed in three intervals: 960 elements in $R_i < R < 0.1\,R_e$, 320 elements in $0.1\,R_e < R < 0.5\,R_e$, and 256 elements in $0.5\,R_e < R < R_e$. We consider the engineering constants $E_1 = 15$, $E_2 = E_3 = 1$, $\mathrm{v}_{12} = \mathrm{v}_{13} = 0.25, \mathrm{v}_{23} = 0.5$, where E and v denote the Young's modulus and the Poisson ratio, respectively, and the subscripts 1, 2, and 3 denote the radial, tangential, and axial directions, respectively. These constants correspond to the elastic constants [10]

$$c_{11} = 900/59 \approx 15.25\,, \qquad c_{12} = 30/59 \approx 0.51\,, \qquad c_{22} = 239/177 \approx 1.35\,. \tag{22}$$

In addition, we use $R_i = 0.001$, $R_e = 1$, $p = 0.1$, the penalty parameters $\delta_e = 10^3$ and $\delta = 10^4$, and the initial candidate $\mathbf{s}_0 = \mathbf{0}$, which corresponds to the undistorted configuration of the disk.

We first investigate the Lagrange multiplier field λ associated with the local injectivity constraint $\det \mathbf{F} \geq \varepsilon > 0$, which is imposed for the St Venant-Kirchhoff model, when $\varepsilon \to 0$. In Figure 1, we plot λ versus the radius R for $\varepsilon = 10^{-1}, 10^{-2}, 10^{-3}, 10^{-5}, 10^{-7}$. We see from this figure that the curves tend to a limit curve as $\varepsilon \to 0$; in fact, the curves corresponding to $\varepsilon = 10^{-5}$ and $\varepsilon = 10^{-7}$ are indistinguishable. This behavior is different from the behavior of the linear counterpart of λ, which becomes unbounded as $\varepsilon \to 0$ [11], and is in good agreement with the analytical results of Aguiar and Rocha [5].

In Figure 2, we compare the results obtained with both the St Venant-Kirchhoff and Mooney-Rivlin models. We show the radial displacement u_r (top left), the radial stretch ν (top right), the determinant of the deformation gradient $\det \mathbf{F} = \nu\,\tau$ (bottom left), and the radial stress (bottom right) versus the radius R in a neighborhood of the inner surface of the disk. Regarding the radial stress, we show P_{rr}, given by (14), for the Mooney-Rivlin model and $P_{rr}^a = P_{rr} - \lambda\,\tau$ for the St Venant-Kirchhoff model, where P_{rr}^a is the total radial stress, which includes the effect of both the constitutive part P_{rr}, given by (13), and the Lagrange multiplier field λ associated with the constraint $\det \mathbf{F} \geq \varepsilon$. The solid lines correspond to results obtained with the Mooney-Rivlin (MR) material for different values of c_{33}. The dashed lines correspond to results obtained with the St Venant-Kirchhoff (StVK) material for different values of ε. We see from Figure 2 that the results obtained with both materials have similarities. For instance, as we move away from the inner radius, $\det \mathbf{F}$ remains either constant or approximately constant, increases sharply, and then increases moderately. In addition, as c_{33} and ε decrease, the results obtained with both materials become very similar. In particular, the case MR $c_{33} = c_{22}/100$ is almost indistinguishable from the case StVK $\varepsilon = 0.001$. These results are in very good agreement with the results reported by Aguiar and Rocha [5], which have formulated the disk problem as a boundary value problem and solved it with a phase-plane technique. This boundary value problem is formulated using the Euler-Lagrange equations of the disk MP and additional necessary conditions that its minimizer must satisfy. In this work, our numerical procedure converges to the minimizer of the disk MP, satisfying these Euler-Lagrange equations and necessary conditions.

5 Conclusions

We have considered the equilibrium of an annular disk that is fixed on its inner surface and is subjected to a uniform pressure on its outer surface. The disk is cylindrically orthotropic and radially reinforced. In the context of the classical linear elasticity, the solution of this problem predicts material overlapping. A way to prevent this unphysical behavior consists of using a constrained minimization theory, which was originally proposed in the context of the classical linear elasticity theory [3] and, recently, extended to the nonlinear elasticity theory [4, 5]. A distinguishing feature of this nonlinear counterpart of the constrained minimization theory is that it yields a bounded Lagrange multiplier field, whereas its linear counterpart yields an unbounded one when $\varepsilon \to 0$ for the

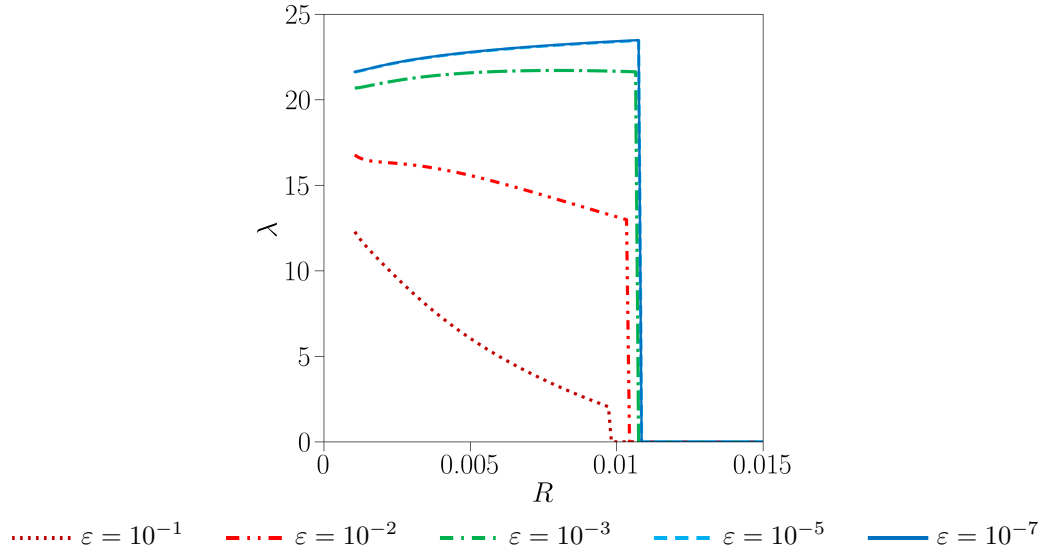

Figure 1. Lagrange multiplier field λ versus R for different values of ε.

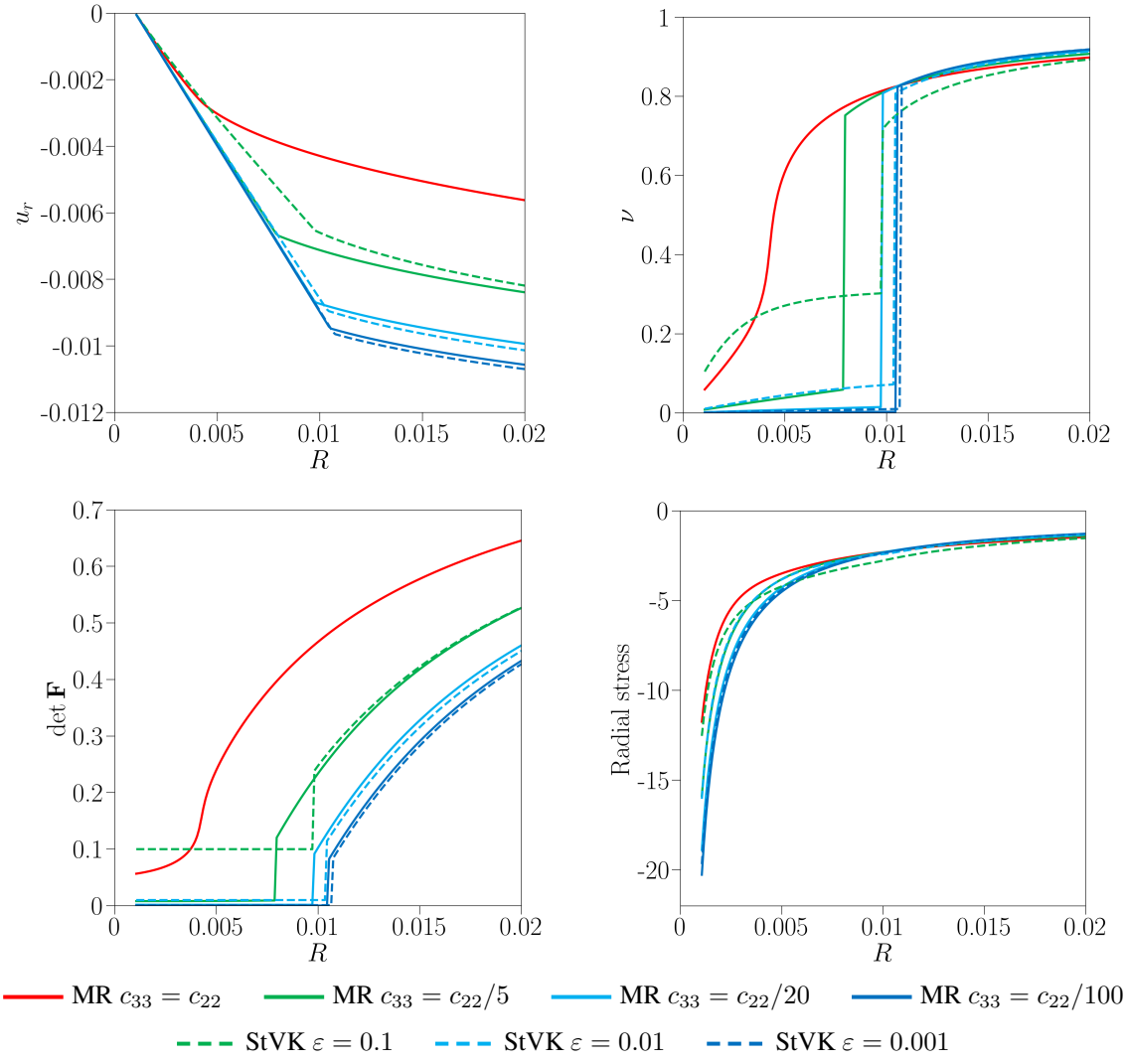

Figure 2. Radial displacement u_r (top left), radial stretch ν (top right), determinant of the deformation gradient $\det \mathbf{F}$ (bottom left), and radial stress (bottom right) versus the radius R for different values of c_{33} and ε.

disk problem. We have also compared the solution obtained by this nonlinear constrained minimization theory with the solution obtained by the standard nonlinear elasticity theory using a model that is conceived to prevent material overlapping implicitly. The solutions obtained from both theories are in very good agreement with each other.

Acknowledgements. The authors acknowledge the support of the National Council for Scientific and Technological Development (CNPq), grant n° 306832/2022-4, São Paulo Research Foundation (FAPESP), grant n° 2022/07083-8, and Coordination for the Improvement of Higher Education Personnel (CAPES) – Finance Code 001.

Authorship statement. The authors hereby confirm that they are the sole liable persons responsible for the authorship of this work, and that all material that has been herein included as part of the present paper is either the property (and authorship) of the authors, or has the permission of the owners to be included here.

References

[1] Forest Products Laboratory. Wood handbook - Wood as an engineering material. Technical report, U.S. Department of Agriculture, Forest Service, Forest Products Laboratory, Madison, 2010.
[2] R. M. Christensen. Properties of carbon fibers. *Journal of the Mechanics and Physics of Solids*, vol. 42, n. 4, pp. 681–695, 1994.
[3] R. L. Fosdick and G. Royer-Carfagni. The constraint of local injectivity in linear elasticity theory. *Proceedings of the Royal Society A: Mathematical, Physical and Engineering Sciences*, vol. 457, n. 2013, pp. 2167–2187, 2001.
[4] A. R. Aguiar and L. A. Rocha. Numerical investigation of orthotropic finite elasticity problem with discontinuous deformation gradient. *Proceedings of the XLIV Ibero-Latin-American Congress on Computational Methods in Engineering*, 2023a.
[5] A. R. Aguiar and L. A. Rocha. On a constrained minimization theory to prevent material overlapping in nonlinear elasticity. *Proceedings of the 9th International Symposium on Solid Mechanics*, 2024.
[6] P. G. Ciarlet. *Mathematical elasticity, volume I: Three-dimensional elasticity*. North-Holand, Amsterdam, 1988.
[7] J. Bonet and A. J. Burton. A simple orthotropic, transversely isotropic hyperelastic constitutive equation for large strain computations. *Computer Methods in Applied Mechanics and Engineering*, vol. 162, n. 1-4, pp. 151–164, 1998.
[8] A. R. Aguiar and L. A. Rocha. Numerical investigation of non-smooth solutions in finite elasticity. In *Proceedings of the 27th International Congress of Mechanical Engineering*, 2023b.
[9] D. G. Luenberger and Y. Ye. *Linear and Nonlinear Programming*, volume 116 of *International Series in Operations Research & Management Science*. Springer US, New York, NY, 2008.
[10] I. M. Daniel and O. Ishai. *Engineering Mechanics of Composite Materials*. Number v. 13 in Engineering mechanics of composite materials. Oxford University Press, New York, 2 edition, 2006.
[11] A. R. Aguiar, R. Fosdick, and J. Sánchez. A study of penalty formulations used in the numerical approximation of a radially symmetric elasticity problem. *Journal of Mechanics of Materials and Structures*, vol. 3, n. 8, pp. 1403–1427, 2008.